Gold nanoparticles deposited on manganese(III) oxide as novel efficient catalyst for low temperature CO oxidation

Lu-Cun Wang, Xin-Song Huang, Qian Liu, Yong-Mei Liu, Yong Cao*, He-Yong He, Kang-Nian Fan, Ji-Hua Zhuang*

Department of Chemistry & Shanghai Key Laboratory of Molecular Catalysis and Innovative Materials, Fudan University, Shanghai 200433, PR China

ABSTRACT

Nanostructured α-Mn$_2$O$_3$ materials have been employed as supports for anchoring gold nanoparticles, which exhibited high activities for low-temperature CO oxidation in the absence or presence of excess H$_2$. The specific activity was found to increase with gold loading up to 5 wt%. Comparing the specific rates for CO oxidation (ca. 1.50 mmol$_{CO}$ g$_{Au}^{-1}$ s^{-1} at 25 °C) with the highly active Au catalysts in the current literature confirmed the exceptionally high activity of these new materials. The rate of CO oxidation showed about half-order dependence of CO partial pressure and was nearly independent of O$_2$ concentration. X-ray photoelectron spectroscopy combined with *in situ* CO adsorption studies revealed the presence of both metallic and positively charged gold species in the catalyst under reaction conditions. As compared with the coprecipitation-derived Au–MnO$_x$ catalyst, the superior activities of Au/α-Mn$_2$O$_3$ have been attributed to its unique redox properties and the facile formation of activated oxygen species on the surface.

© 2008 Elsevier Inc. All rights reserved.

1. Introduction

Catalysts based on supported gold nanoparticles have attracted tremendous recent attention owing to their unique catalytic properties for various oxidation and reduction reactions under mild conditions [1,2]. Studies on Au catalysts have been mainly focused on low-temperature CO oxidation [3], however, for both its simplicity and technological applications in hydrogen purification for fuel cells [3]. In this context, it has been well established that apart from the gold particle size, the choice of support plays a key role in the development of active gold catalysts [3]. Exceptionally high activities for CO oxidation have been reported for finely dispersed Au on reducible oxides, such as TiO$_2$, Fe$_2$O$_3$ and Co$_3$O$_4$ [4]. Recently, CeO$_2$ in its nanocrystalline form was also established as effective support material for Au catalyzed CO oxidation [5]. The essential role of the support is believed to provide oxygen adsorption and activation sites, possibly the oxygen vacancies or reactive perimeter sites at gold–oxide interface, which in turn can afford large amount of highly mobile oxygen species being able to react with CO [3–6].

Based on their superior ability to activate and supply oxygen, manganese oxides (MnO$_x$) have long been used as highly active, durable and low cost catalysts for the combustion of vari-

ous volatile organic substances or hydrocarbons [7–9]. When combined with gold nanoparticles, significantly enhanced activity has been achieved over Au/MnO$_x$ system for low-temperature CO oxidation [10–13] and solvent-free alcohol oxidation [14]. To date, the Au/MnO$_x$ catalysts reported in the literature were mostly prepared by coprecipitation, which however has the disadvantage that the final material is always suffered from the contamination of alkaline metals being notoriously difficult to remove by washing [1,13]. Moreover, the resulting gold particles are mainly embedded in an ill-defined manganese matrix comprising undecomposed manganese carbonates or multivalent manganese oxides. Thus, in most cases, an undesirable high Au loading above ca. 5 wt% is required for achieving a high activity [10–13].

In the present work, we report the development of new efficient manganese oxide supported gold catalyst system exhibiting exceptionally high activity and enhanced stability for CO oxidation in the presence or absence of excess H$_2$ under mild conditions. Single phase manganese(III) oxide (α-Mn$_2$O$_3$), previously established to be an effective material having advantage over its other or multivalent counterparts (MnO$_x$) with better redox properties and structural stability [8,9], has shown to be new attractive supports amenable for the devise of gold-based catalysts highly efficient for low-temperature CO oxidation. Our results have shown that the unique surface redox properties of the Au/α-Mn$_2$O$_3$ system can allow a facile formation of activated oxygen species on the surface, which makes the catalysts highly active and stable for the reaction.

2. Experimental

2.1. Catalyst preparation

Nanostructured α-Mn$_2$O$_3$ was prepared by the direct thermal decomposition of MnCO$_3$ powder (Aldrich) in static air [8]. Different amounts of gold were deposited on the as-synthesized α-Mn$_2$O$_3$ by deposition–precipitation (DP) using urea as the precipitating agent [15]. Typically, 0.55 g of α-Mn$_2$O$_3$ was added to an aqueous solution with the desired amount of HAuCl$_4$ and urea (urea/Au = 100, molar ratio). The suspension was then heated to 90 °C and stirred for 4 h, followed by filtering and washing several times with distilled water to remove the Cl$^-$. The resulting solid product was dried overnight before calcination at 300 °C for 4 h in static air. For comparison, the Au–MnO$_x$ catalyst was prepared by coprecipitation similar to the procedure used by Sanchez et al. [10].

2.2. Catalyst activity tests and kinetic measurements

The catalytic activity tests were performed at atmospheric pressure in a quartz tube micro reactor (i.d. 3 mm). The catalyst weight was 50 mg, and the total flow rate of the reaction gas was 50 mL min^{-1}, with a composition of 1% CO–20% O$_2$ or 1% CO–1% O$_2$–49% H$_2$ (all balanced with He). Before reaction, the catalysts were pretreated with He (30 mL min^{-1}) at 200 °C for 0.5 h. Kinetic measurements were performed under differential reaction conditions, with typically 5 mg catalyst powder. In order to limit the conversion to values typically between 5 and 20%, the catalyst samples were diluted with chemically inert α-Al$_2$O$_3$. Reactions were carried out with a flux of 100 mL min^{-1} at 25 °C in CO and O$_2$ and He as balance. Kinetic data were acquired after 60 min reaction time. The composition of the influent and effluent gas was detected with an online GC-17A gas chromatograph equipped with a TDX-01 column. The conversion of CO was calculated from the change in CO concentrations in the inlet and outlet gases.

2.3. Catalyst characterization

The BET specific surface areas of the samples were determined by adsorption–desorption of nitrogen using a Micromeritics TriStar 3000 equipment. Elemental analysis of the Au loading was performed using ion-coupled plasma atomic emission spectroscopy (ICP-AES) on a Thermo Electron IRIS Intrepid II XSP spectrometer. The X-ray powder diffraction (XRD) of the samples was carried out on a Bruker D8 Advance X-ray diffractometer using nickel filtered Cu$K\alpha$ radiation with a voltage and current of 40 kV and 20 mA, respectively. Transmission Electron Microscopy (TEM) images were recorded on a JEOL 2011 electron microscope operating at 200 kV. Before being transferred into the TEM chamber, the samples dispersed with ethanol were deposited onto a carbon-coated copper grid and then quickly moved into the vacuum evaporator. X-ray photoelectron spectroscopy (XPS) data were recorded with a Perkin Elmer PHI 5000C system equipped with a hemispherical electron energy analyzer. The carbonaceous C 1s line (284.6 eV) was used as the reference to calibrate the binding energies (BE).

The CO adsorption experiments were carried out on a Bruker Vector 22 FT-IR spectrometer equipped with a MCT detector and Harrick diffuse reflectance accessory. *In situ* pretreatment was performed with 30 mL min^{-1} of He at 200 °C for 0.5 h, as in the case of activity measurements. Background signals from gas-phase CO and CO$_2$ were subtracted before the spectra were reported. Temperature-programmed reduction (TPR) profiles were obtained on a homemade apparatus loaded with 20 mg of catalyst. TPR experiments were carried out in 5% H$_2$/Ar flowing at 40 mL min^{-1}, with a ramping rate of 10 °C min^{-1} to a final temperature of 650 °C. The H$_2$ consumption was monitored using a TCD detector. For the titration experiments, the fresh catalysts were switched to a stream of 1% CO/He gas at 25 °C after pretreatment in He at 200 °C for 30 min. The evolution of CO and CO$_2$ concentration was monitored by online mass spectrometer (Balzers OmniStar), which allows detection of CO and CO$_2$ in a helium matrix without interference problems. In the second run, the titrated samples were exposed to oxygen at 80 °C for 30 min, then purged with He before switching back to the CO stream.

3. Results and discussion

3.1. CO oxidation activity and reaction kinetics

Fig. 1a displays the temperature dependence of the CO conversions for various catalysts with nominal gold loadings ranging from 0 to 5 wt%. For the sake of comparison, the activity of 5.5% Au–MnO$_x$ catalyst derived from conventional coprecipitation method is also included. It is clear that the activities of the supported gold catalysts are much higher than that for the pure α-Mn$_2$O$_3$ support material. The temperature at which the conversion was 50% (T_{50}) for α-Mn$_2$O$_3$ is 134 °C (Table 1), which is in good agreement with the literature results under similar conditions [16] and is 125 °C higher than that for the 1% Au/α-Mn$_2$O$_3$ catalyst. Moreover, one can see that complete oxidation of CO could be attained at room temperature over 1% Au/α-Mn$_2$O$_3$, the activity of which is notably higher than that of 5.5% Au–MnO$_x$. Another notable issue from Fig. 1a is the smooth light-off behavior for α-Mn$_2$O$_3$ supported catalysts, in contrast to that on MnO$_x$. Likely, the physical structure of the α-Mn$_2$O$_3$ support is advantageous in avoiding diffusion or mass-transfer limitation. The data in Fig. 1a also indicate that the oxidation activity per catalyst increased monotonously with Au loading for the present samples, with T_{50} decreasing with increased Au loading (Table 1). Similar behavior has been reported for other gold-based catalysts, such as Au/TiO$_2$ [17], Au/CeO$_2$ [18], and Au/Fe$_2$O$_3$ [19].

Table 1

Physicochemical properties and catalytic activities (r_{Au}, T_{50} and E_a) for 5.5% Au–MnO$_x$ and various Au/α–Mn$_2$O$_3$ catalysts with different gold loadings. Reaction conditions: 50 mg catalyst, 1% CO–20% O$_2$ balanced with He, 50 mL min^{-1}

Catalyst	Au loading[a] (wt%)	S_{BET} (m^2 g^{-1})	d_{Au}[b] (nm)	T_{50}[c] (°C)	r_{Au}[d] (mmol$_{CO}$ g$_{Au}^{-1}$ s^{-1})	E_a (kJ mol^{-1})
α-Mn$_2$O$_3$	/	37	/	134	/	37
1% Au/α-Mn$_2$O$_3$	1.0	35	2.7	9	0.41	22
2% Au/α-Mn$_2$O$_3$	1.9	33	2.3	−27	0.81	21
3% Au/α-Mn$_2$O$_3$	3.0	29	2.2	−48	1.50	21
5% Au/α-Mn$_2$O$_3$	4.9	27	3.1	−63	1.74	18
5.5% Au–MnO$_x$	3.6	143	3.3	25	0.10	/

[a] Determined by ICP-AES analysis.
[b] Average gold particle size estimated by statistical analysis from TEM results.
[c] The temperature at which the conversion was 50%.
[d] The specific reaction rate of CO oxidation at low conversions under a kinetically controlled regime at 25 °C.
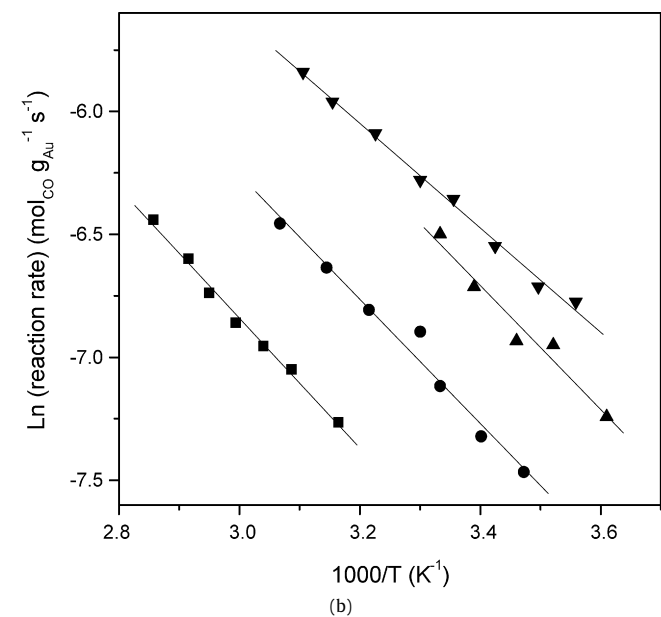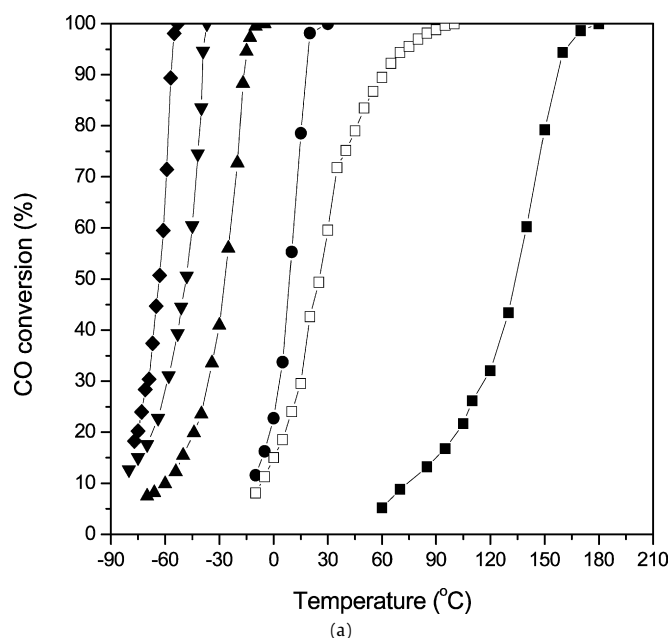
Fig. 1. (a) CO oxidation activity of (□) 5.5% Au–MnOₓ and Au/α-Mn₂O₃ catalysts with different gold loadings: (■) α-Mn₂O₃, (●) 1%, (▲) 2%, (▼) 3% and (◆) 5%. Reaction conditions: 50 mg catalyst, 1% CO–20% O₂ balanced with He, 50 mL min⁻¹. (b) Arrhenius plots of the reaction rate ln(r) vs 1/T for CO oxidation over various Au/α-Mn₂O₃ catalysts. Feed gas: 1% CO–20% O₂ balanced with He, 100 mL min⁻¹. (■) 1%, (●) 2%, (▲) 3% and (▼) 5%.

Fig. 1b presents the reaction rates (r_{Au}) that are normalized to gold mass for these catalyst samples plotted against the reciprocal of the temperature. Presumably, if the activity is dominated by the Au particle size, one would expect a constant Au mass-normalized reaction rate when taking into account the relatively similar gold particle sizes of 2–3 nm (Table 1). However, the data in Fig. 1b and Table 1 evidently shows that increased Au content led to higher Au mass-normalized reaction rate over the range of 1–5 wt%, pointing to different intrinsic activities of the gold nanoparticles in the various samples. As a consequence, it can be deduced that apart from the Au particle size, the gold–support interactions play a vital role in determining the intrinsic activity of Au/α-Mn₂O₃ catalysts. Furthermore, the activation energies (E_a) derived from the plots in Fig. 1b are similar for each of the samples (Table 1), indicating that
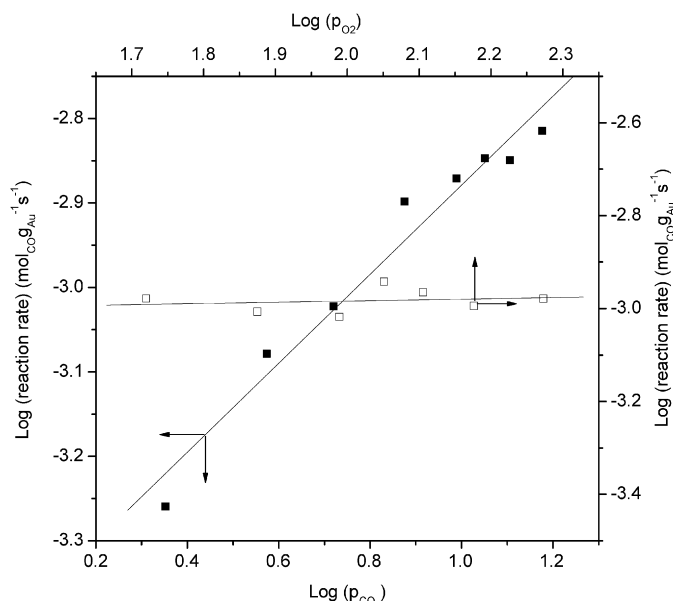
Fig. 2. Determination of the reaction order of CO (0.3–2 kPa CO, 20 kPa O₂, balance He) and O₂ (5–25 kPa O₂, 1 kPa CO, balance He) in a gas flow of 100 mL min⁻¹ at 25 °C over 3% Au/α-Mn₂O₃.

different Au loadings do not change the reaction mechanism of CO oxidation over the gold catalysts. It is apparent moreover that the reaction rate is governed by the pre-exponential term ln A, inferring the presence of a higher population of the active centers in the higher loaded samples. Here it is also interesting to note that only a much smaller difference of the specific rates is identified for the 3% and 5% materials. All these results can be rationalized by assuming that the reaction rate is controlled by the perimeter interface or more precisely the activated "circular zones" around each Au particle [20]. The effective area of these "circular zones" will start to overlap thus reaching a maximum as the Au content rises, which may account for the observed behavior of the Au/α-Mn₂O₃ material.

The reaction order with respect to the two reactants CO and O₂ was determined on the 3 wt% Au catalyst by varying the concentration of the one component in the gas mixture while keeping the concentration of the other constant (Fig. 2). The CO partial pressure was varied between 0.3 and 2 kPa, at 20 kPa O₂ pressure; in another set of measurements, the partial pressure of O₂ was varied from 7 to 25 kPa, at $p_{CO} = 1$ kPa (Fig. 2). The order of the CO oxidation reaction was estimated to be 0.53 with respect to CO and 0.02 with respect to O₂. The published kinetic data for CO oxidation over several typical gold catalysts at similar reaction conditions are summarized in Table 2. It can be seen that there are considerable discrepancies in the literature data with respect to the reaction order of CO and O₂, even for the same catalytic system. This may be caused by the very different experiment conditions. Lin et al. have demonstrated that the CO and O₂ reaction orders over Au/TiO₂ catalyst are strongly dependent on the reaction temperature, partial pressure and catalyst preparation method [21]. In the present study, the near independence of O₂ concentration suggests that the incorporation of oxygen from the feed gas is not rate-limiting step for CO oxidation. Moreover, the relatively lower activation energy over the Au/α-Mn₂O₃ catalyst (Table 2) may be related with the very small gold particle size and intimate metal–support interactions (as shown in the following sections), both of which facilitate the adsorption and activation of the reactants.

In order to compare the catalytic performance of the 3% Au/α-Mn₂O₃ catalyst with other reported gold catalysts in the oxidation

Table 2
Comparisons of kinetic parameters and reaction rates at 25 °C for the CO oxidation over 3% Au/α-Mn$_2$O$_3$ catalyst with other gold catalysts

Catalyst	d_{Au} (nm)	p_{CO}, p_{O_2} (kPa)	E_a (kJ mol^{-1})	r_{Au} (mmol$_{CO}$ g$_{Au}^{-1}$ s^{-1})	TOF[a] (s^{-1})	α_{CO}[b]	α_{O_2}[c]	Ref.
3% Au/Mn$_2$O$_3$	2.2	1.0, 20	21	1.50	0.55[a]	0.53	0.02	This study
3.15% Au/Fe$_2$O$_3$	6.5	1.0, 20	31	0.36	0.30	0.58	0.23	[22]
0.66% Au/Fe$_2$O$_3$	3.6	1.0, air	35	0.18	0.086	0	0.05	[4]
1.2% Au/Co$_3$O$_4$	∼2	1.0, air	16	0.44	0.48	0.05	0.27	[4]
3.3% Au/TiO$_2$	3	1.0, air	34	0.64	0.32	0.05	0.24	[4]
3.1% Au/TiO$_2$	2.9	1.0, air	27	0.64	0.26	n.r.[d]	n.r.	[23]
0.94% Au/Al$_2$O$_3$	2.4	1.0, air	32	0.21	0.02	n.r.	n.r.	[24]
6.6% Au/SiO$_2$	6.6	1.0, air	17	0.05	0.02	n.r.	n.r.	[24]

[a] The turnover frequency (TOF) is calculated on the basis of surface gold atoms estimated by the model of hemispherical ball.
[b] α_{CO}, reaction order of CO.
[c] α_{O_2}, reaction order of O$_2$.
[d] Not reported.
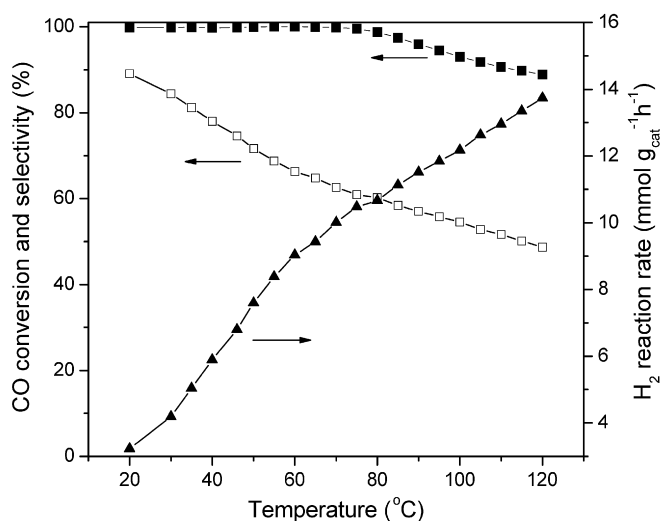
Fig. 3. Preferential oxidation of CO in H$_2$-rich gas over 3% Au/α-Mn$_2$O$_3$. (■) CO conversion, (□) selectivity to CO$_2$ and (▲) H$_2$ oxidation rate. Reaction conditions: 100 mg catalyst, 1% CO–1% O$_2$–50% H$_2$ in He, space velocity 3 × 10^4 h^{-1} mL g$_{cat}^{-1}$.

Fig. 4. CO conversion in PROX as a function of time on stream over 3% Au/α-Mn$_2$O$_3$ (■, □) and Au–MnO$_x$ catalysts (●). Reaction conditions: 100 mg catalyst, 1% CO– 1% O$_2$–50% H$_2$ in He, space velocity 3 × 10^4 h^{-1} mL g$_{cat}^{-1}$, 25 °C.

of CO, the intrinsic activities in terms of the mass-specific reaction rates (mmol$_{CO}$ g$_{Au}^{-1}$ s^{-1}) based on total gold atoms as well as the turnover frequencies (TOF) based on surface gold atoms are also tabulated in Table 2. It is known that the activities of gold catalysts can be greatly influenced by gold particle size, the type of support and reaction conditions [3]. Therefore, comparison of activities for different catalytic systems is usually difficult. However, there are general agreements that small gold particle size is indispensable for its high activity and that gold supported on reducible oxides is more active than gold supported on non-reducible oxides (SiO$_2$, γ-Al$_2$O$_3$) [1]. These conclusions can also be corroborated by the data listed in Table 2. A rough comparison of the mass-specific reaction rate and TOF with other gold catalysts under similar reaction conditions reveals that our catalyst appears to be among the most active Au-based catalysts reported thus far [4,22–25].

3.2. Preferential CO oxidation (PROX) in excess H$_2$

Along with the kinetics of CO oxidation, the 3% Au/α-Mn$_2$O$_3$ catalyst was also tested for PROX in the presence of excess hydrogen. This reaction is of special interest for fuel cell technologies when carried out at low temperatures (20–80 °C) [23,26], as trace amounts of CO are known to poison fuel cell electrodes. The difficulty of this process is to obtain a high rate of reaction while maintaining a very high selectivity for oxidizing CO instead of H$_2$. Fig. 3 shows that CO can be selectively oxidized in H$_2$-rich stream over the Au/α-Mn$_2$O$_3$ catalyst. This behavior is consistent with the

well-known capability of Au being able to oxidize CO more readily than H$_2$ [10], which is a fundamental prerequisite for PROX reaction. It is remarkable that complete removal of CO can be achieved at temperatures as low as 20 °C. At this temperature the oxygen consumption demonstrated a high selectivity up to ca. 90% for CO oxidation. Moreover, over 99.5% of CO conversions could be achieved at temperatures ranging from 20 to 80 °C, with the selectivity to oxygen for CO oxidation higher than ca. 60%. Whereas such PROX performance is comparable with those of the best Au-based catalytic systems reported in the literature [10,26–28], it may be noted that, from a technological point of view, there is still a great challenge to achieve >99.5% CO conversion at around 80 °C with high O$_2$ selectivity. At higher temperatures, both the CO conversion and the selectivity to oxygen gradually decreased due to the competitive oxidation of H$_2$ in the reaction mixture.

One of the most challenging problems faced by gold-based catalysts is the stability on line. To examine the likely long-term behavior of the Au/α-Mn$_2$O$_3$ catalysts under real PROX conditions, an extended on-stream operation for selective CO oxidation in the presence of H$_2$, CO$_2$ and H$_2$O at 25 °C was carried out. As shown in Fig. 4, for PROX reaction in the absence of CO$_2$ and H$_2$O, the catalytic activity is stable for at least 10 h without significant loss of activity and selectivity. CO$_2$ addition leads to a drastic decrease of the activity. This can be reasonably attributed to the accumulation of surface carbonate species, which block the active sites for the PROX reaction [29–31]. However, upon further addition of water, the activity of the catalyst could be improved appreciably. This
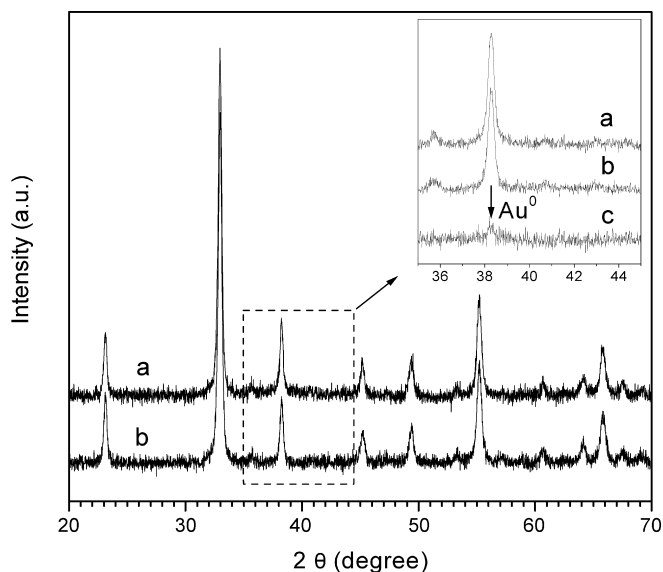
Fig. 5. XRD patterns of (a) α-Mn$_2$O$_3$, (b) 3% Au/α-Mn$_2$O$_3$ and (c) difference spectrum (b)–(a), the arrow indicates the diffraction from gold nanoparticles.

promotion effect has been explained by the fact that water can facilitate the decomposition of the surface carbonate species [31]. The overall effect is that the negative influence of CO_2 is counteracted by the co-addition of water in the reaction feed, demonstrating great potential for practical applications. It is also worthwhile to note that the reference Au–MnO$_x$ catalyst experiences considerable activity decay even at the initial stage of the reaction under "dry" PROX conditions, which is consistent with literature reports [10]. Such significant deactivation has been interpreted by the intrinsic structural instability of the Au–MnO$_x$ system under PROX conditions [32].

3.3. Catalyst characterization

3.3.1. Structural properties and chemical states

The real gold contents of various Au–Mn catalysts were determined by ICP-AES. Results given in Table 1 show that the measured gold content was essentially the same as the nominal loading for all α-Mn$_2$O$_3$ supported gold catalysts, confirming the effectiveness of the urea-mediated Au deposition onto the α-Mn$_2$O$_3$ support [15]. In contrast, the real gold content of the coprecipitation-derived Au–MnO$_x$ catalyst is found to be significantly lower than the nominal value. The as-synthesized α-Mn$_2$O$_3$ has a moderate BET surface area (S_{BET}) of 37 m^2 g^{-1}. When gold was deposited onto the surface of α-Mn$_2$O$_3$, a slightly reduced BET surface area was identified. On increasing the Au loading from 1% to 5%, the surface area of the Au/α-Mn$_2$O$_3$ catalyst decreased monotonously from 35 to 27 m^2 g^{-1}. Of all the Au-loaded catalysts investigated, the coprecipitation-derived Au–MnO$_x$ catalyst shows the highest surface area (ca. 143 m^2 g^{-1}).

The XRD pattern of the as synthesized nanocrystalline Mn(III) oxide support (Fig. 5a) shows well-defined diffraction feature characteristics of α-Mn$_2$O$_3$ (bixbyite, JCPDS 41-1442). After the deposition of gold nanoparticles onto the α-Mn$_2$O$_3$ support, an almost identical XRD pattern was obtained for Au/α-Mn$_2$O$_3$ comparing with α-Mn$_2$O$_3$, indicating a well maintaining of the crystal structure of the nanocrystalline α-Mn$_2$O$_3$ support. Fig. 5b shows the XRD pattern for a typical 3% Au/α-Mn$_2$O$_3$ catalyst. Comparison with the XRD pattern of α-Mn$_2$O$_3$ reveals that most of the reflections stem from the parent support material. No distinct gold reflections are visible in the patterns, owing to the fact that the strongest reflection from polycrystalline gold overlaps with that of
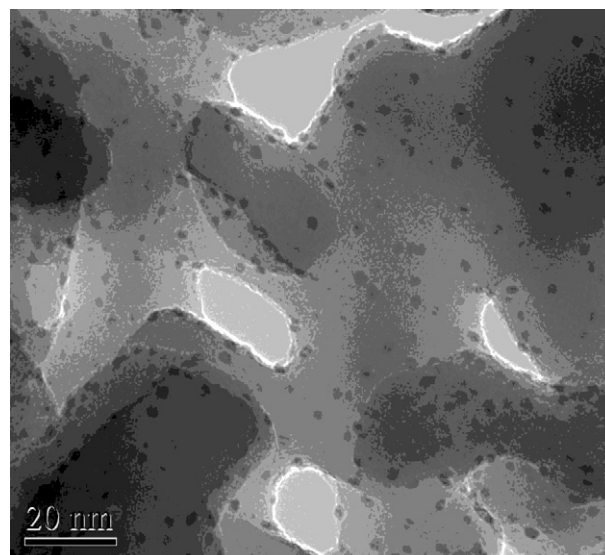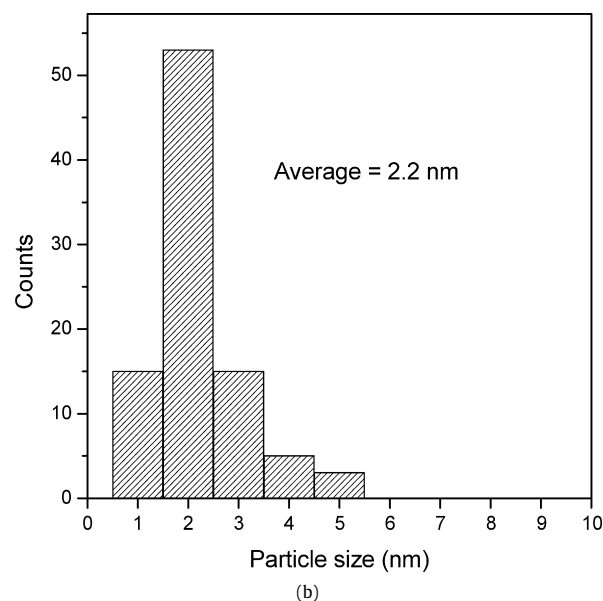
Fig. 6. Representative TEM image (a) and size distribution of gold particles (b) for the 3% Au/α-Mn$_2$O$_3$ catalyst.

α-Mn$_2$O$_3$ at $2\theta = 38.2°$. After subtraction of the pure α-Mn$_2$O$_3$ XRD pattern from that of the Au-loaded sample (inset to Fig. 5), very weak reflections is discernable, as illustrated by the arrow in Fig. 5c. According to Scherrer's equation, crystallite sizes of ca. 2.0 and 20 nm could be estimated for gold nanoparticles and the α-Mn$_2$O$_3$ materials, respectively. TEM analysis reveals that the gold particles are very small and evenly dispersed on the external surface of the α-Mn$_2$O$_3$ support (Fig. 6). The mean particle size was estimated to be ca. 2.2 nm, in good agreement with the XRD results.

The Au 4f XPS spectra of the 3% Au/α-Mn$_2$O$_3$ catalyst before and after CO oxidation are presented in Fig. 7. It should be noted that the XPS peak of Au 4f partially overlaps with that of Mn 3s. As a result, the Au 4f XPS spectra shown in Fig. 7 are those after the Mn 3s component was subtracted [33]. Broad peaks of Au 4f$_{7/2}$ and Au 4f$_{5/2}$ states are identified for both samples, indicating the presence of both metallic and ionic gold species [33,34]. Quantitative deconvolution of the Au 4f peaks resulted in a composition of about 88% metallic and 12% partially oxidized Au species for the fresh catalyst. After CO oxidation reaction, the composition of the

oxidized Au species increased to 20%. These results indicate that two kinds of Au species co-exist in the Au/α-Mn$_2$O$_3$ catalyst. Similar to our findings, the presence of positively charged gold species has also been reported in the Au/CeO$_2$ system even after reductive pretreatment at 200 °C [34]. By using Mössbauer spectroscopy in combination with a range of complementary spectroscopies, Daniells et al. [35] and Hutchings et al. [36] have proposed that cationic gold plays a crucial role in catalyzing CO oxidation over Au/Fe$_2$O$_3$ catalyst. However, the nature of the active gold species during the reaction cannot be established based on the results presented here, since the XPS characterization was made *ex situ*, and a direct correlation between gold species and active sites of the reaction is not valid.
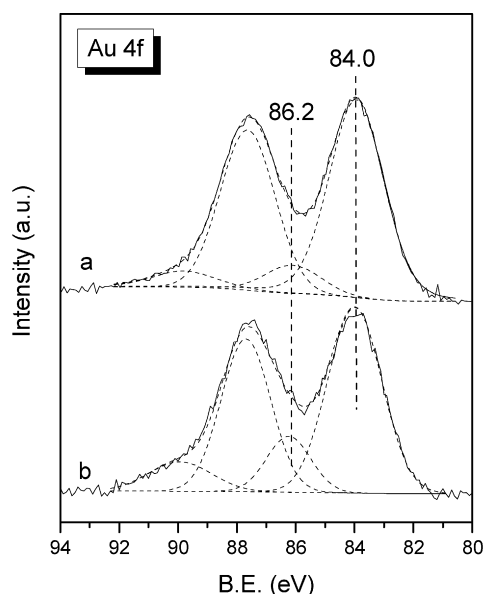
Fig. 7. Au 4f XPS spectra of the 3% Au/α-Mn$_2$O$_3$ catalyst after subtraction of the Mn 3s feature of α-Mn$_2$O$_3$: (a) before reaction, (b) after CO oxidation reaction.

In spite of tremendous research activity over the last decades, the catalytic origin and the very nature of the Au species for CO oxidation are not well understood [37]. Haruta et al. proposed that the reaction takes place at the perimeter of the gold–support interface, i.e., between CO adsorbed on the metallic gold particles (Au^0) and O$_2$ species activated by the oxide support [38]. Bond and Thompson [39] suggested a very similar mechanism involving oxidized gold species (Au^{III}) at the gold–support interface. In contrast, based on a study of CO oxidation over a Au/TiO$_2$(110) model catalyst, Goodman et al. [40] proposed that the reaction occurs only on the small negatively charged gold clusters (Au$^{\delta-}$) with bi-dimensional structures. Moreover, Kung et al. [41] explained the activity of Au/Al$_2$O$_3$ by another mechanism involving the reaction between CO and the Au^I–OH species at the gold–support interface. It appears that the CO oxidation mechanism strongly depends on the type of support, preparation and reaction conditions. The first two mechanisms are especially applicable for gold catalysts supported on reducible oxides.

3.3.2. In situ DRIFT analysis

In situ DRIFT was used to study the adsorption of CO on the calcined catalysts under different conditions (CO atmosphere and CO/O$_2$ mixture) to gain further insight into the exposed Au sites. Fig. 8 shows the DRIFT spectra for CO adsorption on the supported gold catalyst. Prior to CO introduction, the catalyst was *in situ* pretreated in a He stream at 200 °C for 0.5 h. As shown in Fig. 8, the adsorption of CO on 3% Au/α-Mn$_2$O$_3$ led to a strong band at ca. 2107 cm^{-1} with an asymmetric broadening from the high-frequency side. The shape of this absorption band could be well fitted by two components at ca. 2107 and 2124 cm^{-1}. The former band is generally attributed to CO adsorption on the step/kink defect sites of the oxide-supported gold nanoparticles (Au^0–CO) [42,43], while the latter is associated with CO adsorption on positively polarized gold species (Au$^{\delta+}$–CO), which most likely result from the spillover of oxygen or OH groups from the support onto the Au nanoparticles [34,44]. Such CO adsorption bands have also been observed on the Au/TiO$_2$ [45] and Au/CeO$_2$ [5] catalysts under similar conditions. It is also interesting to note that during CO adsorption experiments and without any oxygen in the gas stream,
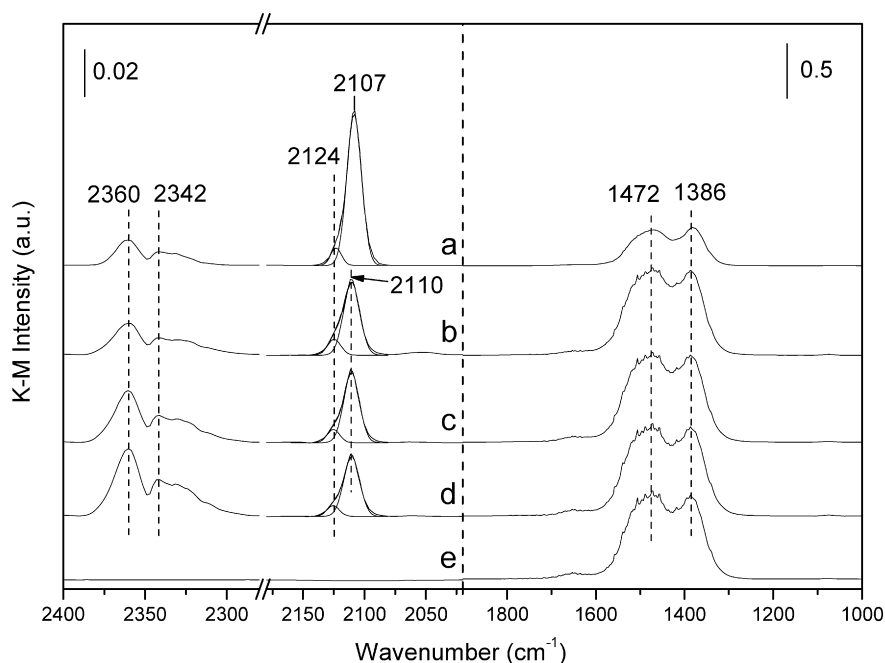
Fig. 8. IR spectra of adsorbed species on 3% Au/α-Mn$_2$O$_3$ (a) 5 min after introduction of 30 Torr of CO, (b) 5 min after successive introduction of 120 Torr of O$_2$, (c) after 30 min, (d) after 1 h, (e) 10 min after evacuation (from the state of (d)) at room temperature. The catalyst was pretreated at 200 °C for 0.5 h in He.
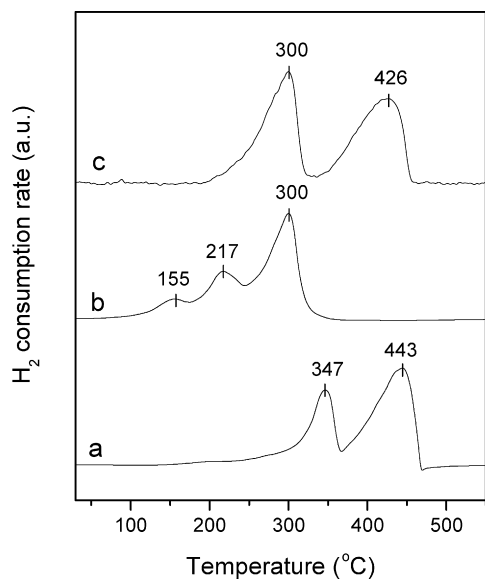
Fig. 9. H_2-TPR profiles of: (a) α-Mn_2O_3, (b) 3% Au/α-Mn_2O_3 and (c) Au–MnO_x.

CO_2 was formed as indicated by the bands at around 2360 and 2342 cm^{-1} [34]. This observation indicates that the α-Mn_2O_3 support is able to supply reactive oxygen to the gold active species for the oxidation of CO. In addition, the presence of CO caused rapid growth of strong bands at 1472 and 1386 cm^{-1} in the carbonate region, corresponding to monodentate and bidentate carbonate species adsorbed on Mn sites [34].

When O_2 was introduced into the CO/He mixture, the intensity of the band due to Au^0–CO decreased notably with the position shifting to 2110 cm^{-1}, while that of the band at 2124 cm^{-1} due to Au$^{\delta+}$–CO remained almost unchanged. The shift of the Au^0–CO band towards high frequency can be reasonably attributed to the decrease of the CO coverage on Au [46,47]. The relative increase of the proportion of the positively charged gold sites is understandable when considering the fact that enough oxygen is present under reaction conditions. This result is also in good agreement with the XPS results where the presence of more cationic gold species was detected on the used catalyst. After 5 min, no further significant change with respect to the intensity of the carbonyl band was observed. Meanwhile, the intensities of the bands due to CO_2 tended to increase with time and those of carbonates quickly reached a steady state; their peak intensities did not increase significantly after 5 min. Evacuation at room temperature for 10 min removed all the bands related to CO and CO_2 adsorption, with the bands of carbonates almost unaltered.

To further understand the effect of Au incorporation on the adsorption properties of the Au/α-Mn_2O_3 system, CO adsorption was also studied on pure α-Mn_2O_3. When exposed to a CO flow, the support materials only showed the doublet of gas phase CO and very weak bands in the region 1800–1100 cm^{-1} due to carbonate species (not shown). After the introduction of O_2, the intensity of the band due to CO_2 appeared and increased to some extent with exposure time. These results are consistent with the broad literature results that Mn_2O_3 can serve as efficient oxidation catalysts by releasing-uptaking oxygen via redox processes [48]. However, it should be noted that the intensities of all adsorption bands on the pure α-Mn_2O_3 are much lower than those on the gold-loaded sample.

In the present work, the foregoing results of DRIFT experiments suggest that gold nanoparticles provide the major CO adsorption sites, which consist of two different kinds of gold species. Moreover, taking into account the E_a of 21 kJ mol^{-1} over Au/α-Mn_2O_3, it can be inferred that CO oxidation mainly occurs at the perime-

ter sites, since the E_a for CO oxidation at step/edge sites of the Au clusters is previously shown to be markedly lower than that at the perimeter sites [1,38]. Furthermore, the adsorption and activation of gas phase O_2 on gold nanoparticles are generally assumed to be very difficult [49], although the dissociation of molecular oxygen has been proposed to occur on ultrathin gold islands or clusters [50]. Accordingly, the positively charged Au species (most likely located at the Au–support interface) indicated by the IR band at 2124 cm^{-1} seems to play a key role in CO oxidation. We speculate that oxygen molecules are adsorbed and activated at the gold–support interface and then transferred to the adjacent gold atoms, where the preadsorbed CO can react with the activated oxygen species to produce CO_2. However, the possibility of adsorption and activation of O_2 directly on the gold species at the perimeter may not be excluded. In a FTIR study of CO oxidation on Au/TiO_2 at 90 K, Boccuzzi and Chiorino have observed a band at 2124 cm^{-1} upon the adsorption of CO on the gold catalyst preadsorbed with $^{18}O_2$ [51]. They proposed that this band could be related to CO adsorbed on gold sites interacting with a superoxidic or peroxidic oxygen molecular species, i.e., O_2^-–Au$^+$–CO, which acts as an intermediate for CO oxidation.

3.3.3. Redox properties and CO titration

TPR experiments were carried out to gain an insight into the redox properties of the Au/α-Mn_2O_3 catalysts. For comparison, the reducibility of the coprecipitation-derived Au–MnO_x catalyst as well as the parent α-Mn_2O_3 materials was also investigated. As shown in Fig. 9, two distinct reduction peaks with similar peak areas were observed for the Au–MnO_x catalyst, corresponding to the stepwise reduction [52] from MnO_2 to Mn_2O_3 (300 °C, 5.59 mmol$_{H_2}$ g^{-1}) and from Mn_2O_3 to MnO (426 °C, 5.50 mmol$_{H_2}$ g^{-1}), respectively. The TPR profile of sample Au/α-Mn_2O_3 shows two peaks at temperatures above 200 °C, with the highest peak maximum (T_M) similar to the first reduction peak of Au–MnO_x catalyst, i.e., 300 °C. A close comparison of the profile for Au/α-Mn_2O_3 sample with those for α-Mn_2O_3 and Au–MnO_x catalysts reveals that the presence of Au nanoparticles strongly promotes α-Mn_2O_3 reduction, as reflected by the significant shift of the reduction maxima (T_M) of the main reduction peak to lower temperatures. Such phenomena may be attributed to the occurrence of spillover effect involving either hydrogen activated on the metal phase or lattice Mn_2O_3 oxygen induced by intimate metal-support interactions [53]. Moreover, in contrast to the doublet reduction feature of α-Mn_2O_3 and Au–MnO_x samples, the Au/α-Mn_2O_3 catalyst show additional low-temperature reduction feature of relatively weak intensity (0.89 mmol$_{H_2}$ g^{-1}) located at ca. 155 °C. This observation, together with the fact that the Au/α-Mn_2O_3 material shows comparable overall H_2 consumption (6.25 mmol$_{H_2}$ g^{-1}) with that for α-Mn_2O_3 sample (6.51 mmol$_{H_2}$ g^{-1}), strongly suggests that the manganese oxide substrates are "activated" to a larger extent in the Au/α-Mn_2O_3 catalyst.

To obtain more information regarding the capability of Au–Mn catalysts to activate oxygen, a CO-titration technique [6] was employed to measure the surface redox properties of the catalyst. Fig. 10 shows the transient response of CO and CO_2 evolution over the two Au-Mn catalysts by switching from pure He to 1 vol% CO in He at room temperature. For Au/α-Mn_2O_3, a sharp and narrow CO_2 peak emerged immediately after exposure to CO, followed by the appearance of a shoulder peak with prolonged exposure time. According to Schubert et al. [6], the first peak could be ascribed to the reaction of CO with the highly reactive oxygen species at the gold–oxide interface, while the second peak may be corresponding to the oxygen species preadsorbed on the support and subsequently migrated to the interface. It is also important to note that the second peak was not observed in previous studies dealing
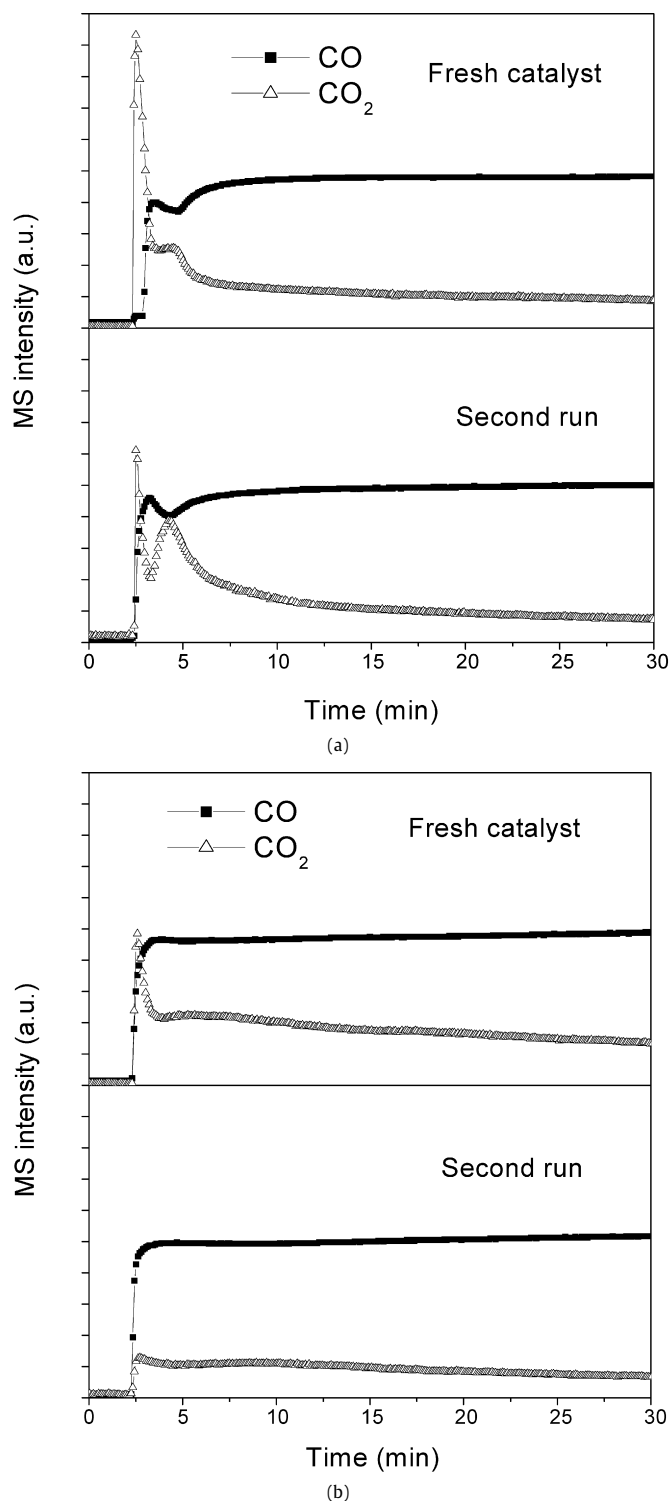
Fig. 10. CO_2 response ($\triangle$) for the reaction of (a) 3% Au/α-Mn_2O_3, (b) Au/MnO_x with respect to CO ($\blacksquare$) exposure. The titration reactions were conducted with 100 mg sample at 25 °C.

with the CO-titration of α-Fe_2O_3 or TiO_2 supported Au catalysts [6,54], inferring an intrinsically different surface redox nature of the Au/α-Mn_2O_3 system. On the other hand, one may notice that similar phenomenon was also observed on Au–MnO_x, with the peak intensity being much weaker than that of Au/α-Mn_2O_3. Furthermore, in the second run of CO titration, the first sharp CO_2 feature is largely retained for Au/α-Mn_2O_3, in sharp contrast to the signal response as detected for Au–MnO_x. These results clearly

demonstrate that Au/α-Mn_2O_3 has a superior capability to activate the molecular oxygen in the reactant gas, leading to the generation of highly reactive surface oxygen species thus significantly enhanced activity in the oxidation of CO.

4. Conclusion

Highly dispersed gold nanoparticles with an average size of ca. 2.2 nm supported on nanostructured α-Mn_2O_3 have been prepared by homogeneous urea deposition-precipitation method. The catalysts are highly active for low-temperature CO oxidation in the presence or absence of excess H_2 and the specific activity was found to increase with gold loading. It was shown that complete CO conversion with very high selectivity (up to 90%) for preferential CO oxidation could be achieved over the Au/α-Mn_2O_3 catalyst in a wide temperature window (20–80 °C), which adds to the most active catalysts for the PROX reaction. As compared with the conventional Au–MnO_x material, the superior activities of the Au/α-Mn_2O_3 system have been attributed to its unique redox properties and the facile formation of activated oxygen species on the surface.

Acknowledgments

References

[1] G.C. Bond, D.T. Thompson, Catal. Rev. Sci. Eng. 41 (1999) 319.
[2] A.S.K. Hashmi, G.J. Hutchings, Angew. Chem. Int. Ed. 45 (2007) 7896.
[3] B.K. Min, C.M. Friend, Chem. Rev. 107 (2007) 2709.
[4] M. Haruta, S. Tsubota, T. Kobayashi, H. Kageyama, M.J. Genet, B. Delmon, J. Catal. 144 (1993) 175.
[5] S. Carrettin, P. Concepción, A. Corma, J.M. Lopez Nieto, V.F. Puntes, Angew. Chem. Int. Ed. 43 (2004) 2538.
[6] M.M. Schubert, S. Hackenberg, A.C. van Veen, M. Muhler, V. Plzak, R.J. Behm, J. Catal. 197 (2001) 113.
[7] G.G. Xia, Y.G. Yin, W.S. Willis, J.Y. Wang, S.L. Suib, J. Catal. 185 (1999) 91.
[8] K. Ramesh, L. Chen, F. Chen, Z. Zhong, J. Chin, H. Mook, Y.F. Han, Catal. Commun. 8 (2007) 1421.
[9] Y.F. Han, L. Chen, K. Ramesh, E. Widjaja, S. Chilukoti, I.K. Surjami, J. Chen, J. Catal. 253 (2008) 261.
[10] R.M.T. Sanchez, A. Ueda, K. Tanaka, M. Haruta, J. Catal. 168 (1997) 125.
[11] S.D. Gardner, G.B. Hoflund, M.R. Davidson, D.R. Schryer, J. Schryer, B.T. Upchurch, E.J. Kielin, Langmuir 7 (1991) 2135.
[12] G.B. Hoflund, S.D. Gardner, D.R. Schryer, B.T. Upchurch, E.J. Kielin, Appl. Catal. B Environ. 6 (1995) 117.
[13] S.J. Lee, A. Gavriilidis, Q.A. Pankhurst, A. Kyek, F.E. Wagner, P.C.L. Wong, K.L. Yeung, J. Catal. 200 (2001) 298.
[14] L.C. Wang, Y.M. Liu, M. Chen, Y. Cao, H.Y. He, K.-N. Fan, J. Phys. Chem. C 112 (2008) 6981.
[15] R. Zanella, S. Giorgio, C.R. Henry, C. Louis, J. Phys. Chem. B 106 (2002) 7634.
[16] S. Imamura, Y. Tsuji, Y. Miyake, T. Ito, J. Catal. 151 (1995) 279.
[17] Y. Tai, K. Tajiri, Appl. Catal. A Gen. 342 (2008) 113.
[18] X.-Y. Wang, S.-P. Wang, S.-R. Wang, Y.-Q. Zhao, J. Huang, S.-M. Zhang, W.-P. Huang, S.-H. Wu, Catal. Lett. 112 (2006) 115.
[19] S. Al-Sayari, A.F. Carley, S.H. Taylor, G.J. Hutchings, Top. Catal. 44 (2007) 123.
[20] F. Moreau, G.C. Bond, Catal. Today 122 (2007) 215.
[21] S.D. Lin, M. Bollinger, M.A. Vannice, Catal. Lett. 17 (1993) 245.
[22] M.M. Schubert, V. Plzak, J. Garche, R.J. Behm, Catal. Lett. 76 (2001) 143.
[23] M.J. Kahlich, H.A. Gasteiger, R.J. Behm, J. Catal. 182 (1999) 430.
[24] G.R. Bamwenda, S. Tsubota, T. Nakamura, M. Haruta, Catal. Lett. 44 (1997) 83.
[25] M. Okumura, S. Nakamura, S. Tsubota, T. Nakamura, M. Azuma, M. Haruta, Catal. Lett. 51 (1998) 53.
[26] P. Landon, J. Ferguson, B.E. Solsona, T. Garcia, A.F. Carley, A.A. Herzing, C.J. Kiely, S.E. Golunski, G.J. Hutchings, Chem. Commun. (2005) 3385.
[27] M. Lomello-Tafin, A.A. Chaou, F. Morfin, V. Caps, J.-L. Rousset, Chem. Commun. (2005) 388.

[28] R.J.H. Grisel, B.E. Nieuwenhuys, J. Catal. 199 (2001) 48.
[29] Y. Denkwitz, Z. Zhao, U. Hörmann, U. Kaiser, V. Plzak, R.J. Behm, J. Catal. 251 (2007) 363.
[30] S.T. Daniells, A.R. Overweg, M. Makkee, J.A. Moulijn, J. Catal. 230 (2005) 52.
[31] M.M. Schubert, A. Venugopal, M.J. Kahlich, V. Plzak, R.J. Behm, J. Catal. 222 (2004) 32.
[32] C. He, H.R. Kunz, J.M. Fenton, J. Electrochem. Soc. 148 (2001) A1116.
[33] S.D. Gardner, G.B. Hoflund, M.R. Davidson, H.A. Laitinen, D.R. Schryer, B.T. Upchurch, Langmuir 7 (1991) 2140.
[34] R. Leppelt, B. Schumacher, V. Plzak, M. Kinne, R.J. Behm, J. Catal. 244 (2006) 137.
[35] S.T. Daniells, A.R. Overweg, M. Makkee, J.A. Moulijn, J. Catal. 230 (2005) 52.
[36] G.J. Hutchings, M.S. Hall, A.F. Carley, P. Landon, B.E. Solsona, C.J. Kiely, A. Herzing, M. Makkee, J.A. Moulijn, A. Overweg, J. Carlos Fierro-Gonzalez, J. Guzman, B.C. Gates, J. Catal. 242 (2006) 71.
[37] G.C. Bond, C. Louis, D. Thompson, Catalysis by Gold, Imperial College Press, London, 2006, p. 189.
[38] M. Haruta, M. Daté, Appl. Catal. A Gen. 222 (2001) 427.
[39] G.C. Bond, D. Thompson, Gold Bull. 33 (2000) 41.
[40] M. Valden, X. Lai, D.W. Goodman, Science 281 (1998) 1647.
[41] M.C. Kung, R.J. Davis, H.H. Kung, J. Phys. Chem. C 111 (2007) 11767.
[42] M. Haruta, Catal. Today 36 (1997) 153.
[43] M.A. Bollinger, M.A. Vannice, Appl. Catal. B Environ. 8 (1996) 417.
[44] F. Boccuzzi, A. Chiorino, S. Tsubota, M. Haruta, J. Phys. Chem. 100 (1996) 3625.
[45] J.-D. Grunwaldt, M. Maciejewski, O.S. Becker, P. Fabrizioli, A. Baiker, J. Catal. 186 (1999) 458.
[46] B. Schumacher, Y. Denkwitz, V. Plzak, M. Kinne, R.J. Behm, J. Catal. 224 (2004) 449.
[47] M.M. Schubert, M.J. Kahlich, H.A. Gasteiger, R.J. Behm, J. Power Sources 84 (1999) 175.
[48] K. Ramesh, L. Chen, F. Chen, Y. Liu, Z. Wang, Y.-F. Han, Catal. Today 131 (2008) 477.
[49] D.C. Skelton, R.G. Tobin, D.K. Lambert, C.L. DiMaggio, G.B. Fisher, J. Phys. Chem. B 103 (1999) 964.
[50] V.A. Bondzie, S.C. Parker, C.T. Campbell, Catal. Lett. 63 (1999) 143.
[51] F. Boccuzzi, A. Chiorino, J. Phys. Chem. B 104 (2000) 5414.
[52] E.R. Stobbe, B.A. de Boer, J.W. Geus, Catal. Today 47 (1999) 161.
[53] H. Trevino, G.D. Lei, W.M.H. Sachtler, J. Catal. 154 (1995) 245.
[54] M. Olea, Y. Iwasawa, Appl. Catal. A Gen. 275 (2004) 35.